Structural Characterization of Semifluorinated *n*-Alkanes. 2. Solid–Solid Transition Behavior

Thomas P. Russell,* John F. Rabolt, Robert J. Twieg, and Richard L. Siemens

IBM Almaden Research Laboratory, San Jose, California 95120

Barry L. Farmer

Washington State University, Pullman, Washington 99164. *Received June 10, 1985*

ABSTRACT: A series of semifluorinated *n*-alkanes, $F(CF_2)_n(CH_2)_mH$, have been observed to undergo a solid–solid phase transition below the crystal melting point. Characterization of this transition has been achieved by a combination of differential scanning calorimetry, Raman spectroscopy, small-angle X-ray scattering, and wide-angle X-ray diffraction. For compounds where $n = 12$ and $m = 2$, 4, or 6 the molecular axes are tilted with respect to the crystal surface normal prior to the transition. For compounds where $n = 12$ and $m = 8$, 10, or 12 evidence for a tilted bilayered crystal structure below the transition temperature was found. The transition involves a translation of the molecules along their axes via a simple screw motion whereupon they enter a rotator phase prior to melting similar to that found in *n*-alkanes.

Introduction

Previously[1] the synthesis and characterization of a series of semifluorinated *n*-alkanes of the form $F(CF_2)_n(CH_2)_mH$ (referred to as F*n*H*m*) were reported. In that study, the room temperature structure and morphology of the F*n*H*m* compounds were discussed and several different molecular packings were proposed. In addition, a preliminary observation of a solid–solid phase transition that occurred at temperatures below the melting point was made. Characterization of the origin and an elucidation of the mechanism of such transitions in these semiflexible compounds are important since they would provide a means of predicting corresponding behavior in their polymeric analogues.

Solid–solid transitions below the melting point have been studied extensively and are well documented for the *n*-alkanes.[2–11] Broadhurst,[11] for example, has presented a comprehensive study and a detailed description of the transition behavior in *n*-alkanes. In addition to changes in the unit-cell structure, the odd-numbered *n*-alkanes were shown to exhibit a rotator phase a few degrees below the melting point. In this structure the molecules maintain their lateral hexagonal packing but rotate about their molecular axes. Additional motions within the crystal, namely defect diffusion and chain twisting, have been discussed by Strobl.[12]

Unlike the case of the *n*-alkanes and polyethylene, perfluorinated model compounds have not been studied because of the limited commercial availability of the high purity, low molecular weight analogues. Consequently, there has been very little structural work reported on model compounds, and the emphasis has been placed instead on the characterization of the homopolymer, poly(tetrafluoroethylene) (PTFE). Even so, the polymer has been the subject of considerable research activity[13–23] due to its unique properties and the presence of multiple solid-state phase transitions.

It is the intent of this work to describe the existence of solid–solid phase transitions in the semifluorinated *n*-alkanes (F*n*H*m*) and to characterize the structure and morphology of these compounds below and above the transition temperatures. Results of calorimetric, spectroscopic, and diffraction studies are used to describe the mechanism by which the solid–solid transition occurs. In addition, the effect of the alkane sequence length on the molecular packing below the transition temperature is discussed.

Experimental Methods

The synthesis and purification of the semifluorinated alkanes used in this study are identical with those described previously.[1] All the F*n*H*m* compounds studied here had a purity in excess of 99%, as determined by gas chromatography.

Differential scanning calorimetry (DSC) measurements were performed on a Du Pont 910 DSC with a 1090 controller. Unless otherwise noted a scanning rate of 1 °C/min was used. Integration of both the solid–solid transition and solid–melt endotherms was accomplished by using standard routines available with the instrument. A sample weight of ca. 10 mg was used for investigation of the solid–solid transitions, whereas 2-mg specimens were used for the melting-endotherm evaluation.

Raman measurements were recorded by using a Jobin-Yvon HG-2S double monochromator configured for photon counting by using a Nicolet 1180 data system. Variable temperature studies were carried out in a specially constructed, doubly insulated, vertical Harney–Miller cell. Helium gas, cooled or warmed in a heat exchanger, was passed over the sample, which had been enclosed in a melting point capillary held in contact with an iron/constantan thermocouple. In this way the sample temperature could be maintained constant to with ±3 °C.

Small-angle X-ray scattering (SAXS) measurements were performed with a Kratky camera using a standard focus Cu tube with Ni filtering. The entire scattering profile was collected by using a TEC Model 210 position-sensitive proportional counter over a period of 24 h. Discrimination of the scattered radiation was achieved electronically. Powder specimens for both SAXS and diffraction measurements were packed within 1-mm-diameter glass capillary tubes having wall thicknesses of 0.01 mm. The capillaries were mounted into a heating cell with mica windows with a hydrocarbon oil to provide thermal contact with the heating block. The temperature of the cell directly outside the capillary tube was monitored with a chromel/alumel thermocouple, and a separate thermocouple was mounted into the heating block to provide a feedback signal for the heaters. Temperature control to within ±3 °C was attained in this manner.

Wide-angle X-ray diffraction patterns were obtained by using a flat plate camera (Warhus) with sample-to-film distances of 50, 170, and 290 mm. Typical exposure times of 3 h were required by the Ni-filtered Cu radiation. Diffraction patterns were obtained at room temperature, at a temperature between the observed solid-state transition temperature and the melting temperature, and again at room temperature to ensure reproducibility. Temperature was controlled to within ±2 °C by using a proportional controller and measured with an iron/constantan thermocouple embedded in the heating block adjacent to the capillary.

Room temperature wide-angle diffraction patterns were also obtained between 5° and 30° 2θ by using an automated powder diffractometer. The observed d-spacings obtained from measurements of the patterns recorded photographically were within ca. 3% of the values measured on the diffractometer.

0024-9297/86/2219-1135$01.50/0

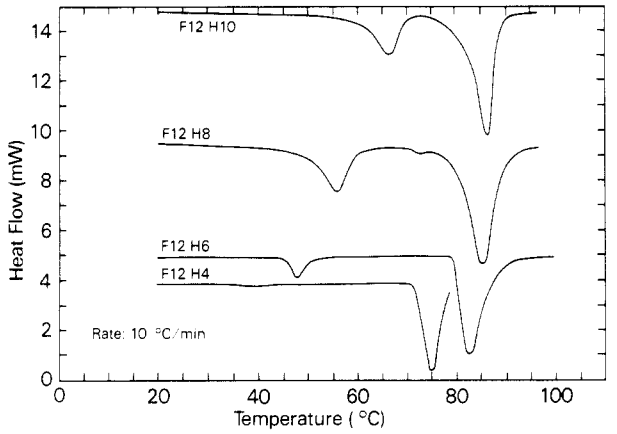

Figure 1. DSC thermograms of some semifluorinated alkanes scanned at a rate of 10 °C/min. The thermograms are labeled by using the nomenclature established in the text.

Table I
Thermal Characteristics of Semifluorinated *n*-Alkanes (F12H*m*)

m	T_t, °C	ΔH_t, J/mol	T_m, °C	ΔH_f, J/mol
0[a]	*b*	*b*	71.3	23.0
2	*b*	*b*	71.0	20.8
4	40	1.4	76.0	20.9
6	44	3.3	79.0	21.8
8	51	5.6	82.0	21.9
10	66	7.5	84.0	22.2
12	80	11.3	89.0	24.5
14[c]	*b*	*b*	86.0	26.0
16	*b*	*b*	90.0	43.1
18	*b*	*b*	92.0	47.8
20	*b*	*b*	96.0	43.4

[a] $F(CF_2)_{12}H$. [b] No transition observed; subscripts t, m, and f denote solid–solid transition, melting, and fusion, respectively. [c] The thermogram for F12H14 shows evidence for a transition, but the transition occurs too close to the melting point to accurately determine T_t and ΔH_t.

Results and Discussion

Thermal Analysis. DSC curves of the semifluorinated *n*-alkanes (F*n*H*m*) are typified by a strong melting endotherm and for $4 \leq m \leq 14$ a broader, weaker endotherm characteristic of the solid–solid phase transition. Typical DSC curves are shown in Figure 1 for several F12H*m* compounds. Data obtained from the DSC curves of F12H*m* (m = 0–20) are compiled in Table I. As reported previously,[1] the melting temperature increases with the length of the alkane sequence and the melting points fall between those of the corresponding *n*-alkanes and perfluorinated *n*-alkanes as might be expected. The heats of fusion, ΔH_f, in contrast, exhibit rather unusual behavior. On a molar basis, ΔH_f for $m = 0$, i.e., $F(CF_2)_{12}H$, was found to be 23.0 J/mol, which is comparable to a value of 23.3 J/mol for the perfluorinated compound, $F(CF_2)_8F$, found in this laboratory and elsewhere.[24] ΔH_f of the F*n*H*m* compounds is depressed to a value of ~21 J/mol as the methylene sequence length increases. ΔH_f increases dramatically to values >40 J/mol for $m \geq 16$. The initial insensitivity of ΔH_f to the addition of methylene units suggests that for $m \leq 14$ the molecular organization of the perfluoro segments prior to melting is similar to that found in the perfluorinated compound. The sudden increase in ΔH_f for $m \geq 16$ reflects a fundamental change in the molecular packing.

Solid–solid transitions were found for the F12H*m* compounds where $4 \leq m \leq 14$. The temperature at which the rate of transition was largest, corresponding to the maximum in the endotherm, was found to increase with the number of methylene units. Unfortunately, the transition temperature for F12H14 was too close to the melting endotherm to analyze quantitatively and, as such, will not be discussed here. The heats associated with the solid–solid transition, ΔH_t, were also found to increase as m increased from 4 to 12. It is interesting to note that extrapolation of ΔH_t to $m = 2$ yields a value of $\Delta H_t = 0$, which corresponds to the absence of a transition in F12H2. It is noteworthy that ΔH_t increases by ~1.05 J/mol as each additional methylene sequence is added. This would suggest that the mechanism of the solid–solid transition does not change dramatically as the length of the protonated segment is increased. In fact, these data would indicate that a single type of motion or mechanism should characterize the transition behavior regardless of the value of m.

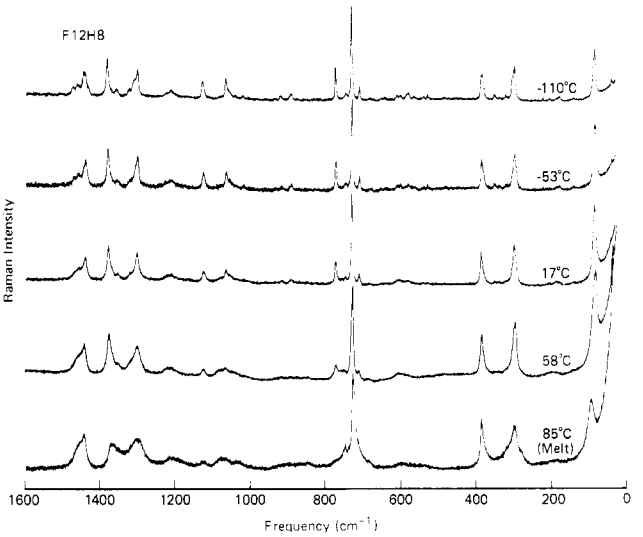

Figure 2. Raman spectra (0–1600 cm^{-1}) of F12H8 at temperatures below and above the solid–solid phase transition. (Resolution = 2 cm^{-1}, 514.5 nm.)

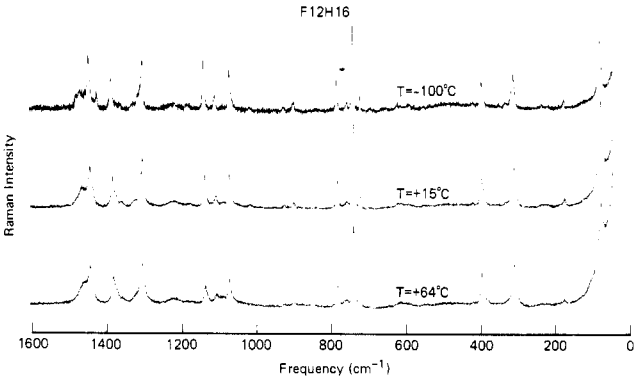

Figure 3. Raman spectra of F12H16 at various temperatures (resolution = 2 cm^{-1}, 514.5 nm). Note the apparent phase transition that is observed in the −100 °C spectrum.

Raman Spectroscopy

Raman studies as a function of temperature were recorded for many of the F12H*m* series, and representative examples are shown in Figures 2 and 3. The spectrum of F12H8 (Figure 2) obtained at 17 °C is typical of that observed for semifluorinated *n*-alkanes; i.e., there is very little overlap between bands associated with either the hydrocarbon or the fluorocarbon segments of the molecule. Thus, the sharp bands in the 200–800-cm^{-1} region and those at 1215, 1296, and 1385 cm^{-1} are attributable to the

vibrations of the fluorocarbon helix, while the remaining medium bands result from vibrations of the $-CH_2-$ sequences. Hence, it is possible to monitor both the helical and planar zigzag conformations of the molecule individually as a function of temperature. This is particularly important in this case where solid–solid phase transitions have been observed.

The very intense low-frequency band observed in the 10–150-cm^{-1} region of Figures 2 and 3 has been assigned[1] to the Raman active longitudinal acoustical mode (LAM) and represents an exception to the above discussion. It has been previously demonstrated that LAM is a composite vibration involving accordionlike motion of the entire backbone. Thus, changes in its frequency reflect changes in molecular length which could occur due to temperature-induced alterations in the conformation of either the helical or trans planar segment.

A number of observations regarding the intermolecular environment of the hydrocarbon segment of F12H8 can be made from Figure 2. As indicated previously,[1] in the 1400–1500-cm^{-1} region are found bands attributable to $-CH_2-$ bending vibrations. Both the number of bands and their relative intensities have been the subject of a number of studies[25] that have correlated this series of bands with the packing symmetry of chains in the crystallographic unit cell. The band pattern observed in F12H8 at 17 °C is indicative of a loose packing of the hydrocarbon segment in a hexagonal structure reminiscent of that observed for the "rotator" phase in n-alkanes.[26] As seen in Figure 2, there is little change in this region at low temperatures with the exception of band sharpening, which reveals several sharp features under the broad band contour observed at 17 °C. Likewise the symmetric (1130 cm^{-1}) and asymmetric (1060 cm^{-1}) CC stretching vibrations characteristic of a trans planar conformation of the $-(CH_2)_mH$ sequence remain fixed but sharpen at reduced temperatures. In addition, the low-frequency LAM vibration appears to be unshifted upon lowering the sample temperature. Its apparent intensity decrease as well as that of other bands in the low-frequency region at −110 °C is due to the temperature dependence of the scattering factor and is unrelated to molecular phenomena.

Increasing the temperature of F12H8 above that of the solid–solid phase transition produces very little change in its Raman spectrum at 58 °C. Of primary significance is the fact that the LAM maintains its frequency position accompanied by a small decrease in intensity. This suggests that the molecule remains fully extended above the crystalline-phase transition, as found previously for the solid-state structure,[27] and implies that the transition itself is associated with a change in the lattice packing without a change in the conformation. This is further supported by the presence of the 1060- and 1130-cm^{-1} bands at 58 °C. It is interesting to note that these bands disappear in the melt phase (Figure 2), as expected, reflecting the random conformation assumed by the $-(CH_2)_mH$ segment above the crystalline melting point. This disorder is further evidenced by the noticeable shift of the LAM vibration to higher frequency in the Raman spectrum at 85 °C. As discussed previously,[27] this is due to the presence of an ordered fluorocarbon segment attached to the disordered hydrocarbon segment, resulting in a net decrease in "effective" chain length. Due to the inverse relationship of frequency and chain length as obtained from the uniform elastic rod model, this chain shortening in the melt phase produces a shift in LAM to higher frequencies.[27]

Quite different spectral behavior with temperature is observed when the length of the hydrocarbon segment exceeds that of the fluorocarbon segment (m = 16, 18, and 20). As mentioned previously, these do not exhibit a solid–solid phase transition above ambient temperature, and, as shown in Figure 3 which contains Raman spectra of F12H16 obtained at −100, 15, and 64 °C, the intensity pattern of the $-CH_2-$ bending region varies remarkably with temperature. At room temperature there is clear evidence of two overlapping bands unlike the asymmetric band profile observed in F12H8 at ambient temperature. In fact, the latter is strikingly similar to that observed in F12H16 at elevated temperature (64 °C). It should be reiterated that the F12H16 does not exhibit a solid–solid phase transition similar to that observed for F12Hm (m = 4–12). In fact, the thermally induced molecular motion in F12H16 at 64 °C is comparable to that found in F12H8 at ambient temperature, suggesting different intermolecular environments of the $-(CH_2)_mH$ segment in these two cases. This is further supported by a comparison of their respective C–H stretching regions (2700–3100 cm^{-1}) and is indicative of a more correlated motion of the hydrocarbon sequence in F12H16 suggestive of a closer packing of the chains at room temperature.

Perhaps a more convincing argument for the uniqueness of the lattice packings found for F12Hm (m = 14–20) is provided by the low-temperature behavior. As seen in Figure 3, in comparison to spectra at temperatures ≥15 °C there are considerable changes observed in the $-CH_2-$ bending region at −100 °C. In addition to the narrowing and upward shift in frequency observed for the high-frequency component, a new band appears at 1415 cm^{-1}. The relative intensity of these three bands is identical with that found for orthorhombic n-alkanes and is strongly suggestive of the existence of an orthorhombic unit cell. DSC measurements indicate the presence of a very weak phase transition in F12H16 in the 0 °C range that may be associated with a change in the unit-cell structure. The low-temperature spectral behavior for F12H16 is in marked constrast to that observed for F12H8, where no such suggestion of an alteration in the unit-cell structure is perceived. As discussed earlier for F12H8, the F12H16 chain length remains unchanged as a function of temperature, as evidenced by the constancy of the observed LAM band.

Small-Angle X-ray Scattering

The general shape of the SAXS profiles depended upon the relative lengths of the protonated and the perfluorinated sequence. For F12Hm where $m \leq 6$, the SAXS consisted of one sharp reflection.[1] With increasing temperature a reflection at smaller angles, i.e., at larger Bragg spacings, emerged. This latter spacing increased while the former decreased. At temperatures above the transition only the reflection corresponding to the larger spacing remained. This is illustrated by the series of SAXS profiles shown in Figure 4 for the F12H4 compound at the temperatures indicated as a function of the scattering vector $h = (4\pi/\lambda) \sin(\epsilon/2)$ where λ is the wavelength and ϵ is the scattering angle. The shape of the scattering profiles changed dramatically for the F12Hm compounds when $6 < m \leq 14$. As shown in Figure 5, three reflections corresponding to two first-order reflections and one second-order reflection were observed at room temperature. As the temperature was increased the intensity of the reflection corresponding to the shorter Bragg distance increased, whereas that for the larger decreased. In contrast to the results for the $m \leq 6$ compounds, only the reflection at shorter distance remained above the transition temperature. It is important to note that at temperatures below the transition temperature two different structures

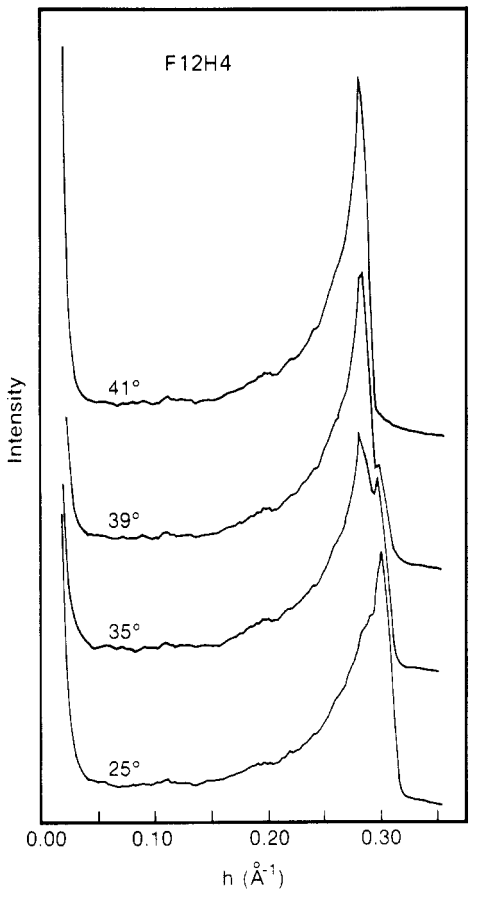

Figure 4. SAXS profiles of the F12H4 compound as a function of temperature (indicated). The individual profiles have been offset vertically for clarity.

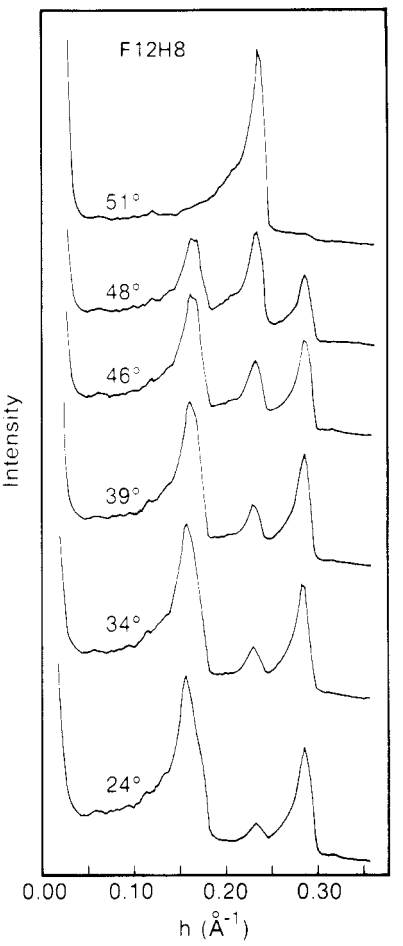

Figure 5. SAXS profiles of the F12H8 compound as a function of temperature (indicated). The profiles at different temperatures have been offset vertically for clarity.

seem to be present over a wide temperature range. Heating the specimen effected an increase in the concentration of the high-temperature structure. These results are consistent with the DSC data where a broad endotherm extending over some 30 °C for the solid–solid transition is observed. The coexistence of two structures or phases is somewhat surprising. Both the SAXS and DSC results are reproducible, and, given the time scales of the SAXS measurements, the compounds, excluding any long term relaxation behavior, should be at equilibrium. Considering the phase rule, over the temperatures where the solid–solid transition occurs, the semifluorinated alkanes are univariant. Consequently, only the temperature of the system needs to be specified in order to define the material thermodynamically.

For $m > 14$ only a single sharp reflection was evident. A second diffuse maximum also appeared at smaller angles for the F12H20 compound. No significant changes in the SAXS were observed for these materials until melting, where all the SAXS vanished with the exception of an angularly independent thermal density fluctuation scattering.

The Bragg spacings corresponding to the first-order maxima are shown in Figure 6 as a function of the alkane sequence length. These data can be grouped into four different categories. First, the dominant low-temperature spacings ($m \leq 6$) are all less than or equal to the fully extended molecular length but increase linearly with m. Second, the stronger low-temperature spacings for $8 \leq m \leq 12$ are proportional to a sum of the length of the alkane segment plus twice the length of the perfluorinated sequence length. Third, the high-temperature spacings for $2 \leq m \leq 14$ are directly proportional to the molecular

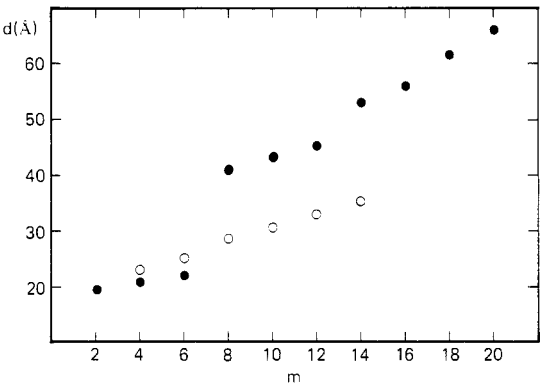

Figure 6. Bragg spacings corresponding to the first-order reflections as a function of the length of the alkane sequence at temperatures below the solid–solid transition temperature (●) and above the transition temperature (○).

length and correspond to the fully extended length of the FnHm molecule. Finally, for $m \geq 14$ the long period increases sharply with m and is somewhat less than twice the molecular length.

In order to describe the angular dependence of the SAXS, model geometries for the packing of the semifluorinated n-alkane stems can be constructed that produce the electron density as a function of distance. Self-convolution of this electron density profile yields the spatial autocorrelation function which is the Fourier transform of the angularly dependent scattering. Comparison of these results with the observed, smeared scattering profiles requires a convolution of the ideal scattering

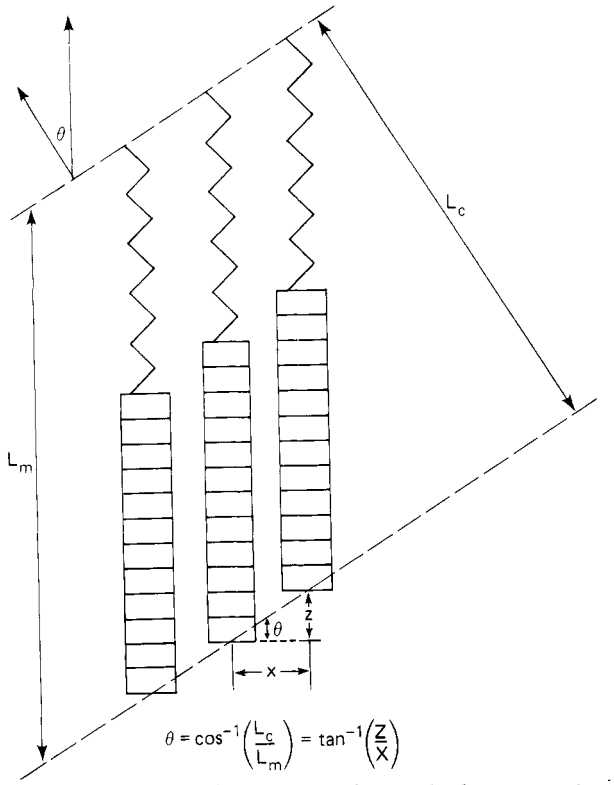

Figure 7. Detailed schematic of a layer tilted at an angle θ, molecular length L_m, and crystal thickness L_c; the zigzag portion of each molecule represents a hydrocarbon segment, whereas the rectangular section represents the fluorinated portion of the molecule. The rectangular subdivisions represent one CF_2 unit.

profile with the slit length weighting function.

Since the Bragg spacing for F12H*m* where m = 2, 4, and 6 is less than or equal to the molecular length, it is evident that the molecular axes must be tilted with respect to the crystal normal. In Figure 7, the tilt angle θ is defined from the length of the molecule L_m and the crystal thickness L_c by

$$\theta = \cos^{-1}(L_c/L_m) \quad (1)$$

Taking into account the fluorine and hydrogen atoms at the ends of each molecule, tilt angles of θ = 0°, 16.6°, and 26.2° for m = 2, 4, and 6, respectively, were determined by assuming that the Bragg spacing in Figure 6 corresponded to L_c. Due to the incorporation of end groups in these calculations, the tilt angles differ slightly from those reported previously.[1] It is evident from Figure 7 that the tilt angle is a function of the intermolecular spacing and the amount of translation of one molecule with respect to its neighbors. Translations along the molecular axis of one and two CF_2 units (1.3 Å each) with a stem separation distance of 5.5 Å yield tilt angles of 13° and 25°, respectively. These values agree with those calculated from the experimental data and indicate that translation of the molecules with respect to one another in multiples of CF_2 units may lead to an optimum packing arrangement.

It was found that both the parallel and antiparallel packing geometries shown in Figure 8a,b could adequately describe the observed SAXS. As the temperature is increased the long period increases to a size equal to that of the fully extended length of one molecule. This can easily be accomplished by translating the molecules along their axes, so that their end groups form a plane perpendicular to the molecular axes.

Several features of this mechanism are appealing. First, as the length of the alkane sequence increases, the energy necessary to bring about the solid–solid phase transition should increase in proportion to the length of the molecule, as observed calorimetrically. Second, the heat of melting would be dominated by the packing of fluorinated segments of the molecule and not by that of the entire F*n*H*m* molecule. Finally, the translation mechanism proposed does not require a large-scale motion of the molecules, in keeping with the low heats of transition.

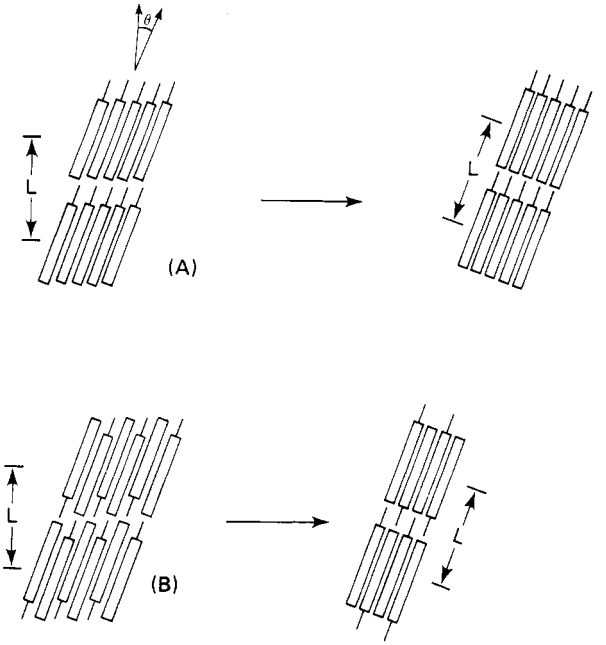

Figure 8. Model for the molecular packing of the F12H*m* compounds where m = 2, 4, and 6. Rectangles represent the fluorinated segments, whereas the solid stems represent the protonated segments. Structure A corresponds to a tilted parallel packing and B to a tilted antiparallel packing. Structures above the transition temperature are located to the right of the arrow. The angle θ is the tilt angle. L corresponds to the distance that would be observed experimentally.

For F12H*m* where m = 8, 10, 12, and 14, the low-temperature Bragg spacings are larger than the lengths of the individual molecules and, consequently, a bilayered structure is necessary in order to describe the scattering. From three dimensional packing considerations, densities derived from diffraction data, the unfavorable interactions between the protonated and fluorinated sequences at lower temperatures, and from the models used to describe the F12H*m* (m = 2, 4, and 6) compounds, several different structures were found to produce scattering profiles similar to those observed. One such model, maintaining the colinearity mandated by the Raman active LAM vibration, is shown in Figure 9. This model basically consists of a tilted bilayer structure. Tilting of the molecular axes by 40.3°, 42.5°, and 44.8° for m = 8, 10, and 12, respectively, is necessary to produce the observed reflections. From the relationship between the tilt angle and molecular translation discussed previously, a translation of four CF_2 units between adjacent molecules is required.

As the temperature is increased, the long period, for m = 8–12, is seen to decrease to a value corresponding to the molecular length. This decrease can occur by translations[28] of the molecules along their axes, yielding the antiparallel packing layered structure shown in Figure 9. The translations required are similar in magnitude to those found for the m = 4 and 6 compounds. It should be kept in mind that the intermolecular distances are dictated by fluorine segment lateral packing, and these helical segments could easily translate past one another by undergoing a screw-type motion, with very little resistance from the hydro-

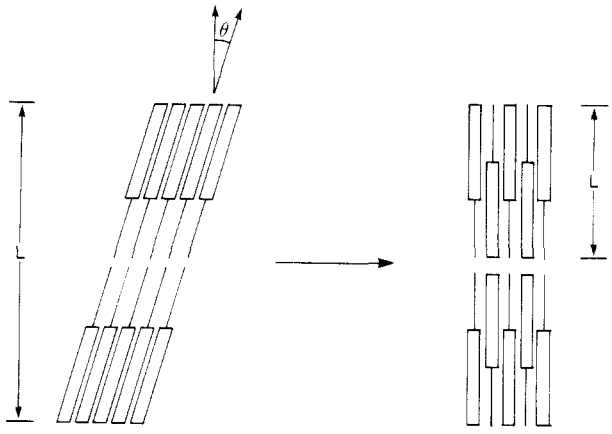

Figure 9. Model for the structure of the F12Hm compounds where m = 8, 10, 12, and 14. Rectangles represent the fluorinated segments, whereas the solid lines represent the alkane segments. This structure corresponds to a bilayer formed by two monolayer crystals of different sizes packing with the alkane sequences adjacent. The structures above the transition temperatures are shown to the right of the arrows. The angle θ is the tilt angle.

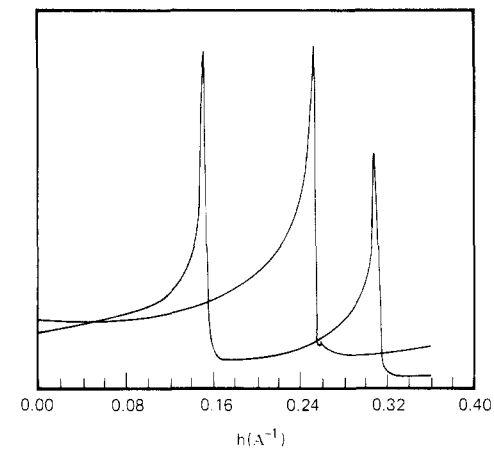

Figure 10. Calculated SAXS profiles for F12H8 below and above the transition temperature. The two profiles were overlaid to emphasize the similarity to the observed SAXS. The scattering profiles calculated for the F12Hm (m = 8, 10, 12, and 14) compounds were similar to that shown here.

carbon segments. In addition, adjacent molecules in the room temperature, tilted-bilayer structure are already translated by one-third (four CF2 units in the F12Hm molecule) of the length of the fluorinated segment. Further translation of the molecules should be facilitated by an increase in temperature.

X-ray diffraction evidence is in keeping with this model, as are the results of limited semiempirical energy calculations. Above the solid–solid transition temperature only one X-ray reflection remained at d = 4.95 Å, indicating a considerable loss of lateral packing order and an increase in the intermolecular separation distances. If the hydrogenated and fluorinated segment lengths are unequal, the lateral spacings must continue to be dominated by the size of the fluorinated segment or else accommodate a volume defect at the end of each molecule to allow close lateral packing of fluorinated and hydrogenated segments. When the fluorinated and hydrogenated segments are virtually the same length (as in F12H12), the random-twisting rearrangement of the molecules leads them to a lateral packing mode, where fluorinated and hydrogenated segments can pack closely together without volume penalty, but the rotational disorder would obviate differences in the diffraction data.

From the proposed models, electron density profiles can be obtained and the SAXS can be calculated. For the model shown in Figure 9, the calculated, smeared SAXS profiles for F12H8 below and above the transition temperature are shown in Figure 10. All of the features of the experimentally observed SAXS profiles are present in the calculated profiles. An exact fitting of the calculated and experimental profiles requires an adjustment of the concentration of each structure. Increasing the temperature corresponds to increasing only the concentration of the high-temperature structure. Similar agreement between the calculated and experimental SAXS was found for the remaining F12Hm compounds. A comparison of the Bragg spacings corresponding to the peak maxima of the experimental and theoretical profiles is given in Table II. Examination of these data shows excellent agreement, in further support of these models.

While some SAXS results on the F12Hm compounds where m > 14 were obtained, a detailed description of the scattering will not be given. The appearance of a diffuse scattering maximum was surprising, but, as discussed in the previous section, the packing geometry appears to change for these compounds. In addition, no solid–solid transitions were observed for these compounds.

Table II
Experimental and Calculated Bragg Spacings[a] for F12Hm

	$T < T_t$		tilt angle,[b]	$T > T_t$	
m	exptl	calcd	deg	exptl	calcd
2	19.7	19.7	0	19.7	19.7
4	20.7	20.7	16.6	22.5	21.6
6	21.8	22.3	26.2	24.8	24.3
8	40.5	40.9	40.3	27.9	26.8
10	42.9	43.2	42.5	30.7	29.3
12	44.9	45.3	44.8	32.9	31.9

[a] All Bragg spacings are given in angstroms and correspond to the first-order reflection. [b] Tilt angles were calculated from eq 1 for $T < T_c$ assuming that L_c corresponded to the experimental Bragg spacing and L_m was equal to the molecular length. For m = 8, 10, and 12 L_m was assumed equal to twice the molecular length.

X-ray Diffraction

Diffraction diagrams of several F12Hm compounds at room temperature are shown in Figure 11. An examination of these data reveals several interesting features. First, the reflection occurring at 2θ = 17.67° (5.01 Å) appears in each profile. The dominance of this reflection, however, diminishes with increasing alkyl sequence length. Secondly, below the solid–solid transition temperature, at least two structures are present in the different materials, as evidenced by the increase in the number of reflections and the appearance of a strong reflection at 2θ = 18.54° (4.78 Å). As the alkyl sequence length increases the diffraction diagrams become more diffuse. For $m \geq 16$ discrete reflections from particular lattice planes are absent and the profiles resemble more amorphous than crystalline materials. This change parallels the spectroscopic and scattering results and indicates a fundamental change in the structure.

Semiempirical energy calculations were undertaken to aid in interpreting the information available from X-ray diffraction experiments and to evaluate possible packing modes. The energy parameters developed by Farmer et al.[30,31] were used to compute the nonbonded interaction energies between fluorine, hydrogen, and carbon atoms in the computer models. The intramolecular geometric parameters, taken from previously used models for polyethylene and PTFE were held fixed. The fluorinated segment was assumed to exist in a 15/7 helical confor-

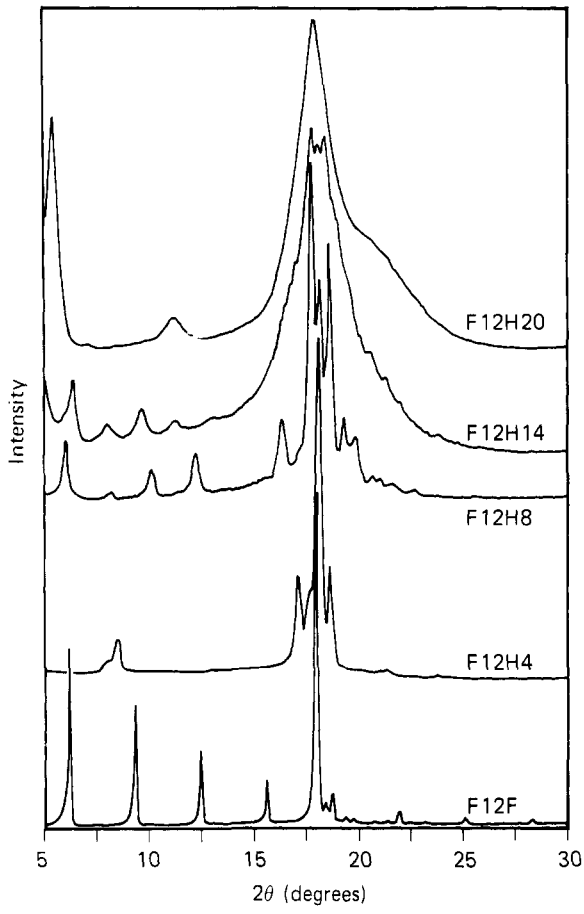

Figure 11. Diffraction diagrams for the F12Hm compounds shown at room temperature. F12F corresponds to $F(CF_2)_{12}F$. The diagrams have been offset vertically for clarity.

mation, and the hydrogenated segment in the usual planar zigzag conformation. In keeping with the spectroscopic LAM results it was assumed that the fluorinated and hydrogenated segments were colinear. Modeling was primarily undertaken for the F12H6 and F12H12 molecules arranged in monolayer structures. Calculations of bilayer structures, focusing particularly on the packing of the end groups at the interface of the layers, have not yet been undertaken.

The energies for parallel and antiparallel packing modes were calculated. For parallel modes, the fluorinated segments greatly dominate the packing. It was found that the lowest energies were obtained when adjacent fluorinated molecular segments were of opposite helical sense, although with only 12 CF_2 units the energetic advantage was substantially less than for that found for PTFE. For antiparallel packing modes, in the F12H12 material, where the fluorinated and hydrogenated segment lengths are very similar, a variety of structures have very similar energies, depending more strongly on the orientations of the hydrogenated segments than on that of the fluorinated segments. For antiparallel packing of F12H6, the fluorine segments dictate the intermolecular distance if molecules are not allowed to translate lengthwise with respect to one another, but the overlapping fluorinated segments are so short as to exert little preference for a particular orientational relationship between adjacent molecules. Translation of the antiparallel molecules to allow a close packing between fluorinated and hydrogenated segments results in the creation of a volume defect at the end of each molecule. This packing defect leads to a considerable increase in the energy. In an attempt to eliminate this energy increase, interdigitated packing structures were examined. However, while there is considerable vacant space, it is not large enough to accommodate another hydrogenated segment without causing so much increased lateral expansion that there is in fact no energy reduction.

Structures examined to find the best packing mode for F12H6 molecules are shown schematically in Figure 12. In every case, the computations were performed strictly on the models shown, and no end-group interactions between layers were considered. Translations of the molecules past one another in the chain axis direction, previously shown to correspond to tilting the molecules within the layer, were not considered in the modeling. Such translations tend to eliminate interactions within one layer which, in a crystal, would be compensated by new interactions with molecules in the adjacent layers.

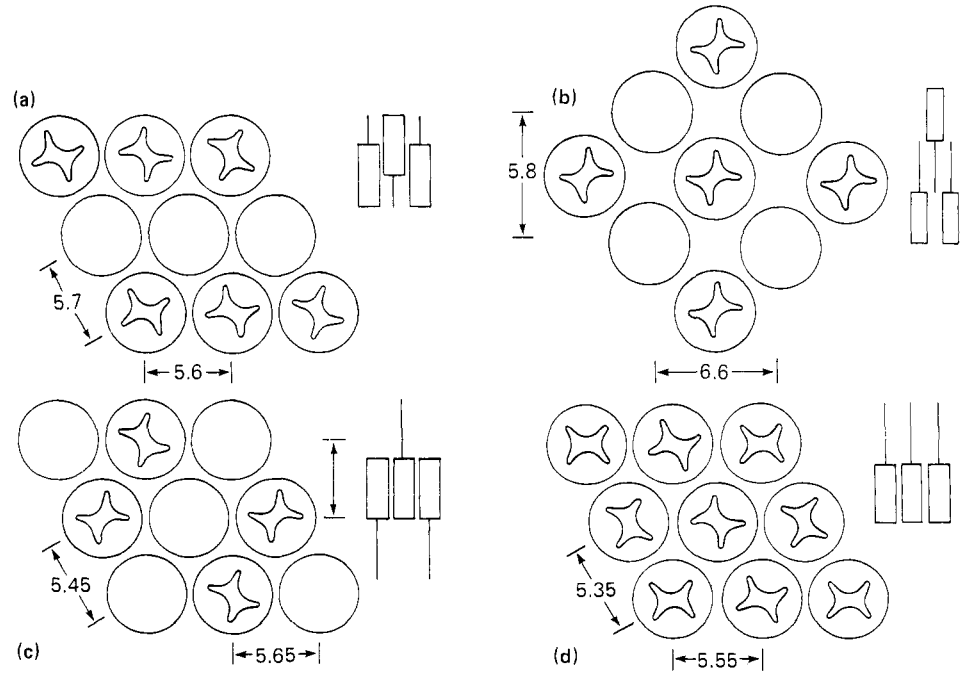

Figure 12. Models used in the packing-energy calculations for F12H6. Details of each are described in the text and in Table III.

Table III
Packing-Energy Calculations

structure	figure	energy, kcal/mol
F12H6		
antiparallel, flush ends	12a	-140
antiparallel, interdigitated orthorhombic hydrocarbons	12b	-107
antiparallel, interdigitated fluorocarbons	12c	-144
parallel, 4 molecules/unit cell	12d	-162
F12H12		
antiparallel, interdigitated orthorhombic hydrocarbons	12b	-165
antiparallel, interdigitated monoclinic hydrocarbons	13a	-172
antiparallel, interdigitated fluorocarbons	12c	-149
antiparallel, flush ends	13b	-190
parallel, 4 molecules/unit cell	12d	-185

The three antiparallel cases examined for the F12H6 packing all gave much higher energies than the parallel packing mode. The energy values, shown in Table III, are those calculated for the nine-molecule arrangements shown in Figure 12. The energy differences between parallel and antiparallel packing modes are of the order of the calculated "heat of sublimation" for an F12H6 molecule. In other words, compared to an eight-molecule model, the energy associated with enlarging the close-packing arrangement to accommodate interdigitation or fluorine segment overlap is about the same as the energy gained by adding the ninth molecule to the model. Clearly, such high cost in energy suggests there would be little tendency for the material to adopt such structures.

The model calculated to have the lowest energy corresponds to the structure typical of that between the solid–solid transition temperature and the melting point. For the reasons cited above, a tilted-structure calculation has not yet been undertaken. However, calculations of the energy as a function of the axial translation between a pair of molecules indicate that only a slight increase in the energy is found for translations up to about 4.5 Å. It is likely that enhanced interactions and optimization of end-group packing could cause the tilted chain structure to be comparable or somewhat lower in energy than the untilted arrangement.

The energies computed for various packing modes for the F12H12 molecules also are listed in Table III, in which reference to the appropriate figure is given for each model. Although additional models for interdigitated structures were considered, the lowest energies were found for noninterdigitated packing arrangements. Parallel packing analogous to the lowest energy structure for F12H6 was again found to be acceptable, but an antiparallel arrangement was found to be somewhat more favorable. Whereas the antiparallel model for F12H6 was not advantageous because of overlap in the fluorinated segments within a layer of dangling hydrocarbon segments too far apart to interact to lower the energy, in the case of F12H12 this antiparallel packing is easily accomplished without either of those difficulties, simply because the hydrocarbon and fluorocarbon segments are virtually the same length.

It is worth noting that either the parallel- or antiparallel-packing modes would give agreement with the most striking feature of the wide-angle X-ray diffraction data. The lateral spacing between antiparallel molecules is 4.8 Å in the minimum-energy structure, and in the parallel arrangement, the spacing between rows of molecules (in contrast to the intermolecular separation distance) is 4.8 Å. Both are in good agreement with the strong observed diffraction maxima between 4.8 and 5.0 Å. Formal determination of the unit cells for these materials has not yet been achieved, and, as such, assignment of the other reflections would be speculative.

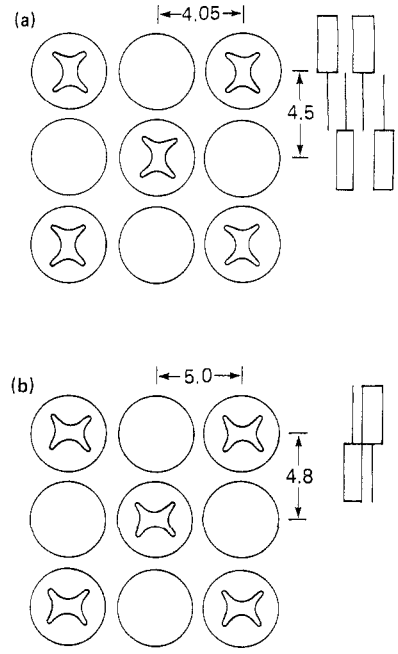

Figure 13. Models used in the packing-energy calculations for the structures for F12H12. Details of each are described in the text and in Table III.

Neither of the low-energy structures calculated is in agreement with the room temperature F12H12 small-angle diffraction data, which indicates a periodicity greater than the molecular length. Modifying the parallel-packing mode by introducing an axial translation of about three CF_2 units leads to a tilted layer with a crystal thickness less than the molecular length. Limited calculations indicate that such translations are energetically reasonable. Consistency with the small-angle data is achieved if such tilted layers are arranged to form a bilayer. Therefore, even though the parallel arrangement yields a slightly higher energy than the antiparallel packing, the interactions between tilted layers must be sufficient to favor a tilted bilayer structure.

Increasing the temperature above the transition temperature substantially alters the overall appearance of the diffraction diagrams. Below the transition temperature spacings corresponding to those seen in Figure 11 are found. Above the transition temperature all but one reflection disappear. This corresponds to a Bragg spacing of 4.95 Å. The absence of reflections other than that attributable to the stem–stem separation distance indicates that the molecules are undergoing motions, most probably rotations about their axes, while maintaining lateral alignment. This resembles the rotator phase[26] observed in the odd-numbered *n*-alkanes or can be likened to a smectic liquid crystalline morphology. In either case, the molecules appear to have a significant amount of mobility above the transition temperature. These motions, however, would be strictly screw rotations and, from the spectroscopic data presented, do not involve the introduction of gauche conformations in the alkane stem.

Conclusions

The solid–solid transition behavior of a series of semifluorinated *n*-alkanes, $F(CF_2)_n(CH_2)_mH$, has been characterized by calorimetric, spectroscopic, and X-ray diffraction techniques. Analysis of the structures above and below the solid–solid transition temperature has shown that the mechanism by which the transition occurs depends upon

the length of the alkyl sequence in relation to that of the perfluorinated segment.

For F12Hm compounds where m = 2, 4, and 6, the structure below the transition temperature was found to consist of crystals where the molecular axes were tilted with respect to the crystal normal. Increasing the temperature effected a translation of the molecules along their axes, producing a structure where the axes were now oriented perpendicular to the surface. Either an antiparallel- or a parallel-packing structure was possible, but semiempirical energy calculations indicated that the latter was more likely. The stable structure below the transition temperature in the m = 8, 10, 12, and 14 compounds consisted of a tilted bilayer structure where the tilt angle is governed by a staggering of the CF_2 units. Above the transition temperature the molecules most likely interleave. In all cases, the mechanism by which the transition occurs was a translation of the molecules along their axes. The high-temperature structure prior to melting was found to be of a rotator phase where the molecules freely rotate about their parallel axes.

Finally, for the F12Hm compounds where $m > 14$ a different structure is evident. The diffraction results clearly indicate that the structure is more diffuse than that for the other semifluorinated alkanes. Dramatic differences in the spectroscopic, diffraction, and thermal data of these compounds support this structural change. Further work is necessary, however, in order to elucidate the precise nature of the crystal packing.

Acknowledgment. We acknowledge several helpful discussions with Professors I. Harrison (Pennsylvania State University) and E. S. Clark (University of Tennessee). We are also grateful to Grace Lim for conducting the powder diffraction experiments. This work was supported, in part, by the National Science Foundation under Grant No. DMR-8419095.

Registry No. $F12H_0$, 66563-68-6; $F12H_2$, 89109-68-2; $F12H_4$, 89109-69-3; $F12H_6$, 89109-70-6; $F12H_8$, 90499-31-3; $F12H_{10}$, 93454-72-9; $F12H_{12}$, 89109-71-7; $F12H_{14}$, 93454-73-0; $F12H_{16}$, 93454-74-1; $F12H_{18}$, 93454-75-2; $F12H_{20}$, 89109-72-8.

References and Notes

(1) Rabolt, J. F.; Russell, T. P.; Twieg, R. J. *Macromolecules* **1984**, *17*, 2786.
(2) Holz, A.; Naghizadeh, J.; Vigren, D. T. *Phys. Rev.* **1983**, *B27*, 512.
(3) Denicolo, I.; Doucet, J.; Craievich, A. F. *J. Chem. Phys.* **1983**, *78*, 1465.
(4) Doucet, J.; Denicolo, I.; Craievich, A. F.; Germain, C. *J. Chem. Phys.* **1984**, *80*, 1647.
(5) Doucet, J.; Denicolo, I.; Craievich, A. F. *J. Chem. Phys.* **1981**, *75*, 1523.
(6) Craievich, A. F.; Denicolo, I.; Doucet, J. *Phys. Rev.* **1984**, *B30*, 4782.
(7) Ungar, G. *J. Phys. Chem.* **1983**, *87*, 689.
(8) Larsson, K. *Nature (London)* **1967**, *213*, 383.
(9) Smith, A. E. *J. Chem. Phys.* **1953**, *21*, 2229.
(10) Crissman, J. M.; Passaglia, E.; Eby, R. K.; Colson, J. P. *J. Appl. Crystallogr.* **1970**, *3*, 194.
(11) Broadhurst, M. G. *J. Res. Natl. Bur. Stand. Sect. A* **1962**, *66A*, 241.
(12) Strobl, G. R. *J. Polym. Sci., Polym. Symp.* **1977**, 59, 121.
(13) Clark, E. S.; Muus, L. T. *Z. Kristallogr.* **1962**, *117*, 119.
(14) Bunn, C. W.; Howells, E. R. *Nature (London)* **1954**, *174*, 549.
(15) Bridgman, P. W. *Proc. Am. Acad. Arts Sci.* **1948**, *76*, 71.
(16) Weir, C. E. *J. Res. Natl. Bur. Stand.* **1951**, *46*, 207.
(17) Beecroft, R. I.; Swenson, C. A. *J. Appl. Phys.* **1959**, *30*, 1793.
(18) Martin, G. M.; Eby, R. K. *J. Res. Natl. Bur. Stand. Sect. A* **1968**, *A72*, 467.
(19) Hirakawa, S.; Takemura, T. *Jpn. J. Appl. Phys.* **1969**, *8*, 635.
(20) Johnson, K. W.; Rabolt, J. F. *J. Chem. Phys.* **1973**, *58*, 4536.
(21) Nakafuku, C.; Takemura, T. *Jpn. J. Appl. Phys.* **1975**, *14*, 599.
(22) Brown, R. G. *J. Chem. Phys.* **1964**, *40*, 2900.
(23) Wu, C. K.; Nicol, M. *Chem. Phys. Lett.* **1973**, *21*, 153.
(24) Campos-Vallette, M.; Rey-Lafon, M.; Lagnier, R. *Chem. Phys. Lett.* **1982**, *89*, 189.
(25) Hendra, P. J.; Jobic, H. P.; Marsden, E. P. *Spectrochim. Acta* **1977**, *A33*, 445.
(26) Barnes, J. D.; Fanconi, B. *J. Chem. Phys.* **1972**, *56*, 5190.
(27) Twieg, R. J.; Rabolt, J. F. *J. Polym. Sci., Polym. Lett. Ed.* **1983**, *21*, 901.
(28) Narang, R. S.; Sherwood, J. *Mol. Cryst. Liq. Cryst.* **1980**, *59*, 167.
(29) Snyder, R. G.; Scherer, J. R.; Gaber, B. P. *Biochem. Biophys. Acta* **1980**, *601*, 47.
(30) Farmer, B. L.; Patel, A., unpublished data.
(31) Farmer, B. L.; Eby, R. K. *Polymer* **1981**, *22*, 1487.

Kinetics of Crystallization in Semicrystalline/Amorphous Polymer Mixtures

G. C. Alfonso† and T. P. Russell*

IBM Almaden Research Center, San Jose, California 95120. *Received October 17, 1985*

ABSTRACT: The kinetics of crystallization in mixtures containing narrow molecular weight fractions of poly(ethylene oxide) (PEO) and poly(methyl methacrylate) (PMMA) have been investigated as a function of the composition and molecular weight of each component and the crystallization temperature. The radial growth rates of the spherulites have been described by a kinetic equation that incorporates the cooperative diffusion coefficient, the thickness of the crystalline lamellae, and the free energy for the formation of secondary crystal nuclei. Adjusting for an apparent molecular weight dependence of the lateral and fold surface free energies of the PEO crystals permitted the construction of a master curve from the growth rate of all the mixtures studied. A precise evaluation of the equilibrium melting point of the PEO crystals in the pure polymer and in the mixtures was hindered by annealing during crystallization and heating. This latter result casts serious doubts on the determination of an interaction parameter via a melting point depression analysis in these mixtures.

Introduction

The addition of an amorphous polymer to a semicrystalline polymer can have dramatic effects on the thermodynamic and kinetic parameters governing the crystallization. From a thermodynamic viewpoint, specific interactions in the mixture lead to a slight depression in the equilibrium melting point[1-3] and a change in the free energy for the formation of nuclei on the crystal surface.[4,5] The kinetics of crystallization are reduced by a dilution of the crystallizable component at the growth surface.[4-6] An important parameter that is modified by mixing and has significant ramifications on the overall mobility in the

†Permanent address: Istituto di Chimica Industriale, Università di Genova, 16132 Genova, Italy.

0024-9297/86/2219-1143$01.50/0